Published online 3 October 2017 *Nucleic Acids Research, 2017, Vol. 45, No. 21* **12325–12339**
doi: 10.1093/nar/gkx881

PARP2 controls double-strand break repair pathway choice by limiting 53BP1 accumulation at DNA damage sites and promoting end-resection

Alexis Fouquin[1,2,3], Josée Guirouilh-Barbat[4], Bernard Lopez[4], Janet Hall[5], Mounira Amor-Guéret[1,2,3] and Vincent Pennaneach[1,2,3,*]

[1]Institut Curie, PSL Research University, UMR 3348, 91405 Orsay, France, [2]CNRS, UMR3348, Centre Universitaire, Bât. 110, 91405 Orsay, France, [3]Université Paris Sud, Université Paris-Saclay, UMR 3348, 91405 Orsay, France, [4]Université Paris Sud, Institut de Cancérologie Gustave Roussy, CNRS UMR8200, 94805 Villejuif, France. Team labeled by la Ligue contre le cancer 'Ligue 2017' and [5]Centre de Recherche en Cancérologie de Lyon, INSERM, CNRS, UMR 1052-5286, 69424 Lyon, France

Received June 28, 2017; Revised September 14, 2017; Editorial Decision September 19, 2017; Accepted September 25, 2017

ABSTRACT

Double strand breaks (DSBs) are one of the most toxic lesions to cells. DSB repair by the canonical non-homologous end-joining (C-EJ) pathway involves minor, if any, processing of the broken DNA-ends, whereas the initiation of DNA resection channels the broken-ends toward DNA repair pathways using various lengths of homology. Mechanisms that control the resection initiation are thus central to the regulation to the choice of DSB repair pathway. Therefore, understanding the mechanisms which regulate the initiation of DNA end-resection is of prime importance. Our findings reveal that poly(ADP-ribose) polymerase 2 (PARP2) is involved in DSBR pathway choice independently of its PAR synthesis activity. We show that PARP2 favors repair by homologous recombination (HR), single strand annealing (SSA) and alternative-end joining (A-EJ) rather than the C-EJ pathway and increases the deletion sizes at A-EJ junctions. We demonstrate that PARP2 specifically limits the accumulation of the resection barrier factor 53BP1 at DNA damage sites, allowing efficient CtIP-dependent DNA end-resection. Collectively, we have identified a new PARP2 function, independent of its PAR synthesis activity, which directs DSBs toward resection-dependent repair pathways.

INTRODUCTION

Deoxyribonucleic acid (DNA) double strand breaks (DSBs) are one of the most toxic lesions to cells. If unrepaired or misrepaired, DSBs result in cell death or in genome instability, which could contribute to cancer development. Repair of DSBs by the canonical non-homologous end-joining (thereafter referred to as canonical end-joining or C-EJ) pathway involves minor, if any, processing of the broken DNA-ends and requires the Ku70/80 complex (Ku) and DNA-PKcs (1). Binding of DSBs by Ku (2,3) and by 53BP1 in complex with its partner RIF1 and PTIP which coordinate the action of Rev7 (4–11) all facilitate C-EJ by preventing DNA end-resection by nucleases.

In contrast, the initiation of DNA resection channels the broken ends towards homology or microhomology-mediated repair. This process is initiated by the MRE11-RAD50-NBS1 complex (MRN) together with CtIP, resulting in the formation of a 3′-single-stranded DNA (ssDNA) stretch (12–15). The DSBs can then be processed by homologous recombination (HR), single strand annealing (SSA), alternative-end joining (A-EJ) or microhomology-mediated template switching (MMTS) pathways (16–19).

When central key C-EJ proteins, such as Ku70/80 or ligase IV are not functional, the DSBs are channeled to the A-EJ pathway after relatively short stretches of broken end-resection (16,17,20). The A-EJ is completed by the sealing of the break with the possible use of DNA sequence microhomology requiring the activity of poly(ADP-ribose) polymerase 1 (PARP1), polymerase θ and DNA ligase I and III (21). In contrast extensive resection, catalyzed by the EXO1, DNA2 and BLM proteins (11,22–24), is required for channeling the repair towards HR (25,26,27). The RPA complex that protects the ssDNA stretch generated by resection is replaced by RAD51, forming a nucleofilament in preparation for the subsequent homology search and strand invasion steps of HR (27). When strand invasion cannot occur or fails, the annealing of two complementary sequences that present some homology, leads to repair by SSA (12,17,28).

The C-EJ and HR pathways are both essentially conservative, whereas the A-EJ, SSA and MMTS pathways will in-

*To whom correspondence should be addressed. Tel: +33 169863105; Fax: +33 169075327; Email: vincent.pennaneach@curie.fr

exorably produce deletions and eventually insertions at the junction of the repaired DNA ends. Therefore, understanding the mechanisms which regulate DNA end-resection and control the appropriate channeling of broken DNA ends towards conservative or mutagenic repair, is of prime importance (1).

The synthesis of polymers of ADP-ribose (PAR) is catalyzed by members of the poly(ADP-ribose) polymerases (PARP) protein family of which the activities of PARP1, PARP2 and PARP3 increase in response to DNA strand breaks (29–31). The PARP catalytic inhibitors currently used in the clinic or under development target both PARP1 and PARP2 because of the remarkable conservation in the structure of their catalytic domain (32). This high degree of similarity could in part explain the functional redundancies between the two proteins, in spite of the large differences in respective levels of enzymatic activity (29). Indeed, PARP1 and PARP2 are equally important in suppressing genomic instability in response to DNA damage (33), facilitating the repair of single-strand breaks (SSBs) (34) and restarting stalled replication forks (35). They also play redundant functions in suppressing T-cell lymphoma (36). However, PARP1 is preferentially activated by DNA nicks and DSBs, whereas PARP2 is predominantly activated by DNA gaps, flaps and recombination intermediates (37–40). Based on these DNA binding specificities it might be expected that PARP1 and PARP2 play different roles in DSB repair (DSBR).

PARP1 has been shown to be involved in the repair of DSB by the A-EJ pathway (41) and PARP3 promotes repair of DSB by the C-EJ pathway (30,42), however there is less direct evidence for an involvement of PARP2 in DSBR. For instance PARP2 expression is induced by mitomycin C in cervical cancer and by radiation and doxorubicin in hepatocarcinoma where it correlates with larger and more aggressive tumors (43,44). In addition, PARP2, but not PARP1 depletion, results in sensitivity to the DSB inducing agent neocarzinostatin (45) and PARP2 specifically protects against illegitimate IgH/c-myc recombination during class switch recombination in mice (46). Taken together these observations suggest that PARP2 may be involved in DSBR, and prompted us to investigate the potential role of PARP2 in DSB repair by HR, SSA and EJ in human cell lines.

We present results highlighting an unsuspected strategic role for PARP2 in orienting the choice of DSBR pathways. We found that PARP2 limits 53BP1 accumulation at the site of DSB, thus favoring CtIP-dependent DNA end-resection. PARP2, together with BRCA1, enhances HR, SSA and A-EJ dependent DSBR. Moreover, the PAR synthesis activity of PARP2 is not required for its function in the DSBR pathway choice.

MATERIALS AND METHODS

Plasmid constructs

The eGFP-PARP-2, GFP-53BP1 and DsRed-Isce1 expression plasmids were a kind gift from Dr V. Schreiber (UMR7175CNRS, ESBS, Illkirch, France), D. A. Friedl (Angewandte Physik und Messtechnik LRT2, UniBW, Germany) and Dr A. Carreira (UMR3348, Institut Curie, Orsay, France) respectively. The eGFP-C1-FLAG-Ku70, eGFP-C1-FLAG-Ku80, eGFP-C1-FLAG-XRCC4 were obtained from Addgene (references #46957, #46958 and #46959). The eGFP-PARP-2 E545A protein (37) was obtained by mutation of the pe*GFP-PARP2* plasmid using the QuikChange II XL Site-Directed Mutagenesis Kit (Agilent) and verified by sequencing. The eGFP-PARP2 was rendered resistant to the siRNA PARP2#1 by introduction of silent mutations at the following nucleotide (5′-CTGATTCA**ATTGCTG**GAAGATGAT-3′).

Cell lines and transfection

The HF cell line is the simian virus 40 (SV40)-transformed derivative of AS3 primary fibroblasts isolated from a healthy donor (47). The HF EJ-CD4 cell line (clone GC92) used to analyse EJ efficiency, is a derivative of the SV40-transformed GM639 human fibroblast cell line, containing the end-joining substrate (pCOH-CD4), as previously described (11). The HF DR-GFP cell line (clone RG37) used to analyse HR efficiency, is a derivative of the SV40-transformed GM639 human fibroblast cell line, containing the homologous recombination (HR) substrate (pDR-GFP), as previously described (48). The human bone osteosarcoma epithelial cell line U2OS DR-GFP (49) was used to analyse HR efficiency. The U2OS-SSA line (19) was used to analyse SSA efficiency. HeLa cell line silenced for BRCA1 (HeLa shBRCA1 was from Tebu-Bio (ref. 00301-00041) and the HeLa cell line silenced for PARP1 (HeLa shPARP1) was previously described in (45). All cell lines were grown at 5% CO_2, 37°C in Dulbecco's modified Eagle's medium (DMEM) supplemented with antibiotics and 10% FCS. All tissue culture reagents were from ThermoFisher Scientific. Bleomycin was obtained from the Institut Curie hospital, the PARP inhibitor Veliparib (also known as ABT-888) was purchased from ENZO Life Science. For protein depletion, cells were transfected with 20 nmol of the targeting siRNA with Interferin (Ozyme, France) according to the manufacturer's instructions. Gene-specific siRNAs for PARP2 (#1 5′-CUAUCUGAUUCAGCUAUUA-3′, #2 5′-GGUUACCAGUCUCUUAAGA-3′ and #3 5′-GACCAACACUAUAGAAACC-3′), for PARP-1 (#1 5′-GAAAGUGUGUUCAACUAAU-3′ and #2 5′-GGGCAAGCACAGUGUCAAA-3′), for BRCA1 (5′-GGAACCUGUCUCCACAAAG-3′), for CtIP (5′-GCUAAAACAGGAACGAAUC-3′), for XRCC4 (5′-AUAUGUUGGUGAACUGAGA-3′), for 53BP1 (5′-AGAACGAGGAGACGGUAAUAGUGGG-3′), for RIF1 (5′-AGACGGUGCUCUAUUGUUA-3′) and negative control siRNA (SR-CL000-005) were obtained from Eurogentec. Plasmids were transfected with Jet-PEI (Ozyme, France) according to the manufacturer's recommendations.

Cell lysates, immunoblotting and immunofluorescence microscopy

Whole cell extracts were prepared by resuspending the cells in 50 mM Tris–HCl pH 7.5, 20 mM NaCl, 0.1% SDS, 1mM $MgCl_2$,10 mM β-glycerol phosphate and 1 mM sodium vanadate containing 50 U/ml of the DNase Benzonase (Merk Millipore) and protease inhibitors cocktail 1 (Sigma-Aldrich) and incubated at 4°C for 20 min. The solubilized

proteins were separated from the cell debris by centrifugation, denatured in Laemmli loading buffer and separated on SDS-PAGE gels. The protein contents were analysed by western blotting using the Odyssey reagents and imaging system (LI-COR Biosciences) according to the manufacturer recommendations.

For protein immunofluorescence staining, cells were grown on glass coverslips. When cells were treated with bleomycin prior to immunostaining, the treatment at a final concentration of 25 μg/ml was performed for 2 h in culture medium. For recovery, the cells were washed with drug-free medium and further incubated for the indicated time into drug-free media. The cells were washed in PBS then soluble proteins were pre-extracted for 5 min on ice in 20 mM NaCl, 300 mM sucrose, 3 mM $MgCl_2$, 10 mM Hepes pH 7, 1 mM EGTA, 0.5% Triton X-100 and fixed in 4% paraformaldehyde at room temperature. Prior to performing the immunostaining, the cells were incubated for 10 min with 0.2% Triton X-100 in PBS and blocked for 30 min in BSA 5%. Primary antibody incubations were done overnight at 4°C. After three washes with 0.5% Triton X-100 in PBS, cells were incubated with appropriate Alexa-labeled secondary antibody (Molecular Probes) for 2 h at room temperature. Cells were washed three times with 0.5% Triton X-100 in PBS and DNA was counter-stained with 0.1 ug/ml 4′,6-diamidino-2-phenylindole (DAPI) in PBS before mounting in fluorescent mounting medium (DAKO). Images were taken using a large field Leica 3D microscope at the 63× objective (Leica microsystem). Antibodies used in this study were: anti-53BP1 (Abcam 21083), anti-RAD51 (Santa Cruz, H-92), anti-RIF1 (Santa Cruz, N-20), anti-γH2AX (Upstate, clone JBW301), anti-RPA32 (Abcam 2175), anti-Ku80 (Abcam 33242), anti-BRCA1 (Santa Cruz, D-9), anti-PARP-1 (Enzo, C2-10), anti-PARP-2 (Enzo, ALX-804-639), anti PAR (Enzo, 10H; Trevigen, 4436-BPC), anti-XRCC4 (Abcam 145), anti-CtIP (Santa Cruz, T-16), anti GFP (Roche Life Sciences, mouse monoclonal), anti-Actin (Thermo Fisher, Ab5), anti-CD4 (BD clone RM4-5).

Flow cytometry

Cell cycle analysis was performed by collecting the cells followed by an overnight fixation in 70% ethanol at –20°C. Cells were rehydrated in PBS containing 0.25% Triton X-100 for 15 min and incubated in PBS containing 25 μg/ml propidium iodide and 25 μg/ml RNase for 15 min at 37°C. For flow cytometry analysis at least 30 000 cells were acquired using a FACScalibur (BD Biosciences) and data were processed using the FlowJo software (FlowJo, LLC). Quantification of RPA accumulation at the chromatin according to the cells DNA content was performed as previously described (50).

Live-cell microscopy and laser micro-irradiation

Laser micro-irradiation experiments were essentially performed as described previously (45) with some modifications. Briefly, the cells were grown on plastic μ-Dish 35 mm (Ibidi) and transfected with the eGFP fusion protein expression plasmid 48 hours prior to imaging. The cells were presensitized by adding 10 μg/ml of Hoechst dye 33258 to the medium for 5 min at 37°C. The recruitment and the real-time follow-up of the protein of interest was carried out using a Confocal Leica SP5 system equipped with a 37°C heating chamber attached to a DMI6000 stand using 63×/1.4 objective of the PICT-IBiSA Orsay Imaging facility of Institut Curie. DNA photodamage were locally induced using a 2-photon laser set to minimal power at 810 nm and focused onto a single spot of constant size (176 nm) within the nucleus to generate a point of photodamage. When indicated, recruitment of the protein of interest was followed for 10 min using a 488 nm argon laser line. The fluorescent protein enrichment at the photodamage site was extracted with the ImageJ software using an in house developed macro (45). Experiments were performed at least three times for each protein of interest.

DNA repair assay

The following cell lines were used to monitor efficiency of I-Sce1 induced DNA DSB repair: the HF EJ-CD4 (clone GC92) was used to analyse end-Joining efficiency, the HF DR-GFP (clone RG37) line and the human bone osteosarcoma epithelial cell line U2OS DR-GFP were used to analyse HR efficiency and the U2OS-SSA line was used to analyse SSA. DNA repair analysis is performed as follows, one day before transfection with siRNA, 1.5×10^5 cells were plated in 60 mm petri dish. After two days, the cells were then transfected with the pDsRed-ISce1 plasmid. Cells were collected after a further 48 hours incubation. The GFP positive cells for the DR-GFP and the SSA cell lines were scored by flow cytometry (FACS calibur, BD Biosciences). For the EJ assay performed in the HF EJ-CD4 line, cells were fixed in 2% paraformaldehyde for 15 min and blocked with 5% BSA in PBS for 30 min. Cells were incubated for 45 min with an 0.5 ug of an anti-CD4 coupled to FITC in 5% BSA/PBS. The cells were washed in PBS before CD4 positive evens were scored by flow cytometry. The relative repair efficiency was determined by correcting the proportion of GFP or CD4 positive cells for the transfection efficiency deduced from the fraction of DsRed positive cells in each sample.

DNA sequence analysis of EJ events

Genomic DNA from HF EJ-CD4 was extracted from frozen cell pellets following DNA repair experiments and PCR amplified with Herculase II Polymerase (Agilent Technologie) using the primers CMV-5 ‘ATTATGCCCAGTA CATGACCTTATG’ and CD4int ‘GCTGCCCCAGAAT CTTCCTCT’ flanking the junction point. The PCR products were gel purified and cloned into the pCR II-Blunt-TOPO vector (Thermo Fisher Scientific) and sequenced (GATC Biotech). Events are categorized in two classes according to the DNA sequence found at the repair junction. The events limited to the 3′Pnt are repair events for which the sequence at the repair junction includes at least one of the four nucleotides from the 3′ Pnt generated by I-SceI cleavage. The events with deletion exceeding the 3′Pnt, are events for which the sequence at the repair junction have four or more of the nucleotides at the I-SceI cleavage site that have been deleted.

Colony formation assay

Cells were transfected with siRNAs, incubated for 48 hours and then trypsinised, counted. For bleomycin treatment, the cells in suspension were supplemented with medium containing bleomycin at the indicated concentration and incubated for 1 hour at 37°C. Following drug dilution, cells were seeded at 1000 cells per well in six-well culture plates in triplicate. The cells were fixed with ethanol 96% after 7 days, and stained with Coomassie blue R250 (0.05%). Colonies of more than 20 cells were counted. Irradiations were carried out at room temperature using low-energy Philipps MCN-323 X-ray generator (200-kVp, 0.3-mm copper and 1-mm aluminum additional filtration, 80-keV effective energy) operating at 21 mA with a dose rate of 1 Gy/min.

Statistical analysis

Unless stated otherwise, statistical analysis performed in the manuscript are standard two-tails t-test performed using the Graphpad PRISM software. $*P < 0.05$; $**P < 0.01$; $***P < 0.001$ and ns, not significant.

RESULTS

PARP2 depletion alters DSB repair efficiency

To investigate the role of PARP2 in the response to DSB, we constructed an SV40-transformed human normal fibroblast cell line (HF) stably expressing a short hairpin RNA (shRNA) to downregulate PARP2 (HF shPARP2) (45). The cells were irradiated with X-rays and treated with the radiomimetic drug bleomycin, both of which generating SSBs and DSBs (51). Compared to the control cell line (HF shcontrol), PARP2 depleted cells (HF shPARP2) were significantly more sensitive to both X-rays (Figure 1A) and bleomycin (Figure 1B). These results indicate a role of PARP2 in both SSBs and DSBs processing.

Next, we determined whether PARP2 could contribute directly to the repair of a single I-Sce1-induced DSB in intrachromosomal reporter substrates. We used three cellular models in which the I-Sce1-cut is a substrate for HR (HF DR-GFP and U2OS DR-GFP cell lines), or for C-EJ and A-EJ (HF EJ-CD4 cell line) (see Supplementary Figure S1A and B and Materials and Methods section for detailed cell lines' description) (11,48,49). We first investigated whether PARP2 could modulate the efficiency of HR. PARP2 silencing with three different siRNAs (Figure 1C and Supplementary Figure S1G) resulted in a significant decrease in HR relative efficiency in both HF DR-GFP (Figure 1D) and U2OS DR-GFP (Figure 1E) cell lines when compared to the control siRNA treated cell lines. We then evaluated the role of PARP2 in EJ repair. We observed that silencing of PARP2 in the HF EJ-CD4 cells, with each of the three siRNAs, resulted in a significant increase in EJ relative efficiency compared to the control siRNA treated cells (Figure 1F). In comparison, PARP1 silencing with two different siRNAs (Supplementary Figure S1F and G) did not alter neither HR relative efficiency in HF DR-GFP and U2OS DR-GFP cells, nor EJ relative efficiency in HF EJ-CD4 cells, compared to control siRNA treated cells (Supplementary Figure S1C-E). Given that siPARP2#1 had the greatest effect on EJ relative efficiency (Figure 1F), that siPARP1#1 gave the strongest knockdown efficacy (Supplementary Figure S1F and G) and siPARP2#1 and siPARP1#1 increased the relative frequency in γ-H2AX foci formation after bleomycin (Supplementary Figure S1H) without affecting the cell-cycle distribution (Supplementary Figure S1I), they were used for all subsequent experiments. Taken together, these results suggest a specific role for PARP2 for promoting HR and inhibiting EJ during DSBR.

PARP2 promotes HR and A-EJ, independently of its PARylation activity

In response to DNA damage, PARP1 produces approximately 85% of the overall cellular PARylation (29). Efforts to identify PARP-specific PARylation targets have revealed that PARP1 and PARP2 have both common and specific modification targets (52,53). To address whether the PARylation activity of PARP2 was necessary for DSBR regulation, we treated both HF DR-GFP and HF EJ-CD4 cell lines depleted of PARP1 with 10 μM of the PARP inhibitor Veliparib which suppressed PAR synthesis activity in presence of damaged DNA (Supplementary Figure S1J and K). We found that treating the PARP1 depleted cells with Veliparib had no effect on HR (Figure 2A) and EJ (Figure 2B) relative efficiencies. In addition, we observed that the Veliparib treatment had no effect on the HR and EJ efficiencies in the siControl treated cells nor in the PARP2 depleted cells (Figure 2A and B). These results suggest that the role of PARP2 in modulating DSBR is independent of its PARylation activity and that PARP1 activity does not affect DSBR either in the presence or in the absence of PARP2.

To directly test this possibility, the HF EJ-CD4 cells were stably transfected with a construct expressing either the GFP fused full-length wild type PARP2 protein (GFP-PARP2) or the PAR synthesis mutant PARP2 E545A protein (GFP-PARP2 E545A) (Supplementary Figure S2A-B). We confirmed that the E545A mutant has no detectable PARylation activity ((37) and Supplementary Figure S2C), and that both the wild type and the PARylation E545A mutant proteins were readily recruited to the site of laser microirradiation induced DNA damage ((54) and Supplementary Figure S2D). We found that PARP2 silencing by siRNA sensitized HF EJ-CD4 cells to bleomycin, and the reintroduction of either the siPARP2 resistant wild type PARP2 or PARP2 E545A mutant fully restored the survival efficiency of PARP2 depleted cells, to the level of control cells (Figure 2C), suggesting that PARP2 facilitates DSB repair independently of its PARylation activity. In addition the reintroduction of the wild type form or the PARylation dead mutant of PARP2 fully restored the relative EJ efficiency in HF EJ-CD4 cells ($P = 0.0018$ and $P = 0.0016$, respectively, Figure 2D). These results allowed us to rule out possible off-targets effect of the siRNAs and to confirm that PARP2 inhibits EJ and promotes cell survival upon DNA damage independently of its PARylation activity.

Interactions between PARP2 and the Ku heterodimer have been reported *in vivo* (52,55,56), thus we next examined if PARP2 could limit C-EJ efficiency by hindering the accumulation of the core EJ proteins at DNA damage sites. We

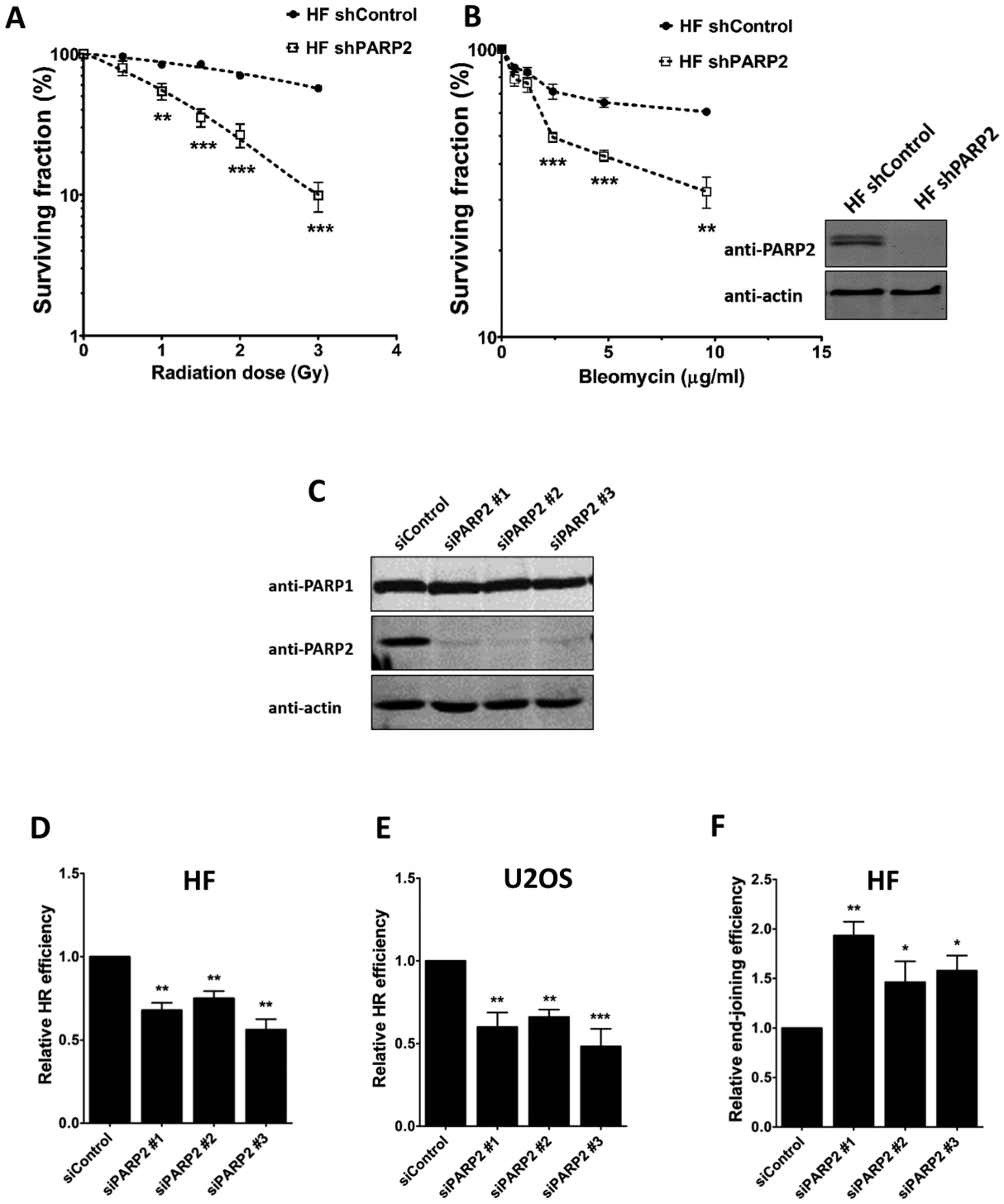

Figure 1. PARP2 depletion alters DSB repair efficiency. (**A**) Effect of PARP2 stable depletion on X-rays induced cytotoxicity measured using a clonogenic surviving assay. The analysis was performed in control SV40-immortalized human fibroblast (HF shcontrol) and in the PARP2 stably depleted cells (HF shPARP2). Each treatment was repeated three times in quadruplicate. Data represents the mean ± SEM. $^{**}P < 0.01$; $^{***}P < 0.001$ (Mann-Whitney test). (**B**) Clonogenic cell survival of HF shControl or HF shPARP2 cells in response to bleomycin. Cells in suspension were exposed to the indicated bleomycin concentration for 1 h before plating in drug-free media. Each treatment was repeated four times in triplicate. Data represents the mean ± SEM. $^{**}P < 0.01$; $^{***}P < 0.001$ (Mann–Whitney test). The expression level of the PARP2 protein in the different cell cultures was assessed by western blotting. (**C**) Western blot analysis of whole cell extracts from HF EJ-CD4 cells transfected with the indicated siRNA. Cells extracts were prepared 48 h post siRNA transfection, corresponding to the I-SceI transfection time point. The relative repair efficiency by HR of I-SceI-induced double strand cut is decreased when PARP2 is depleted in (**D**) HF DR-GFP cells and (**E**) U2OS DR-GFP cells. (**F**) The relative repair efficiency by EJ of I-SceI-induced double strand cut is increased when PARP2 is depleted in HF EJ-CD4 cells. Values plotted represent relative repair efficiency calculated as a ratio of repair efficiency measured in cells transfected with siControl. Values are mean ± SEM from five (HF DR-GFP cells), six (U2OS DR-GFP cells) and five (in HF EJ-CD4 cells) independent experiments. $^{*}P < 0.05$; $^{**}P < 0.01$; $^{***}P < 0.001$.

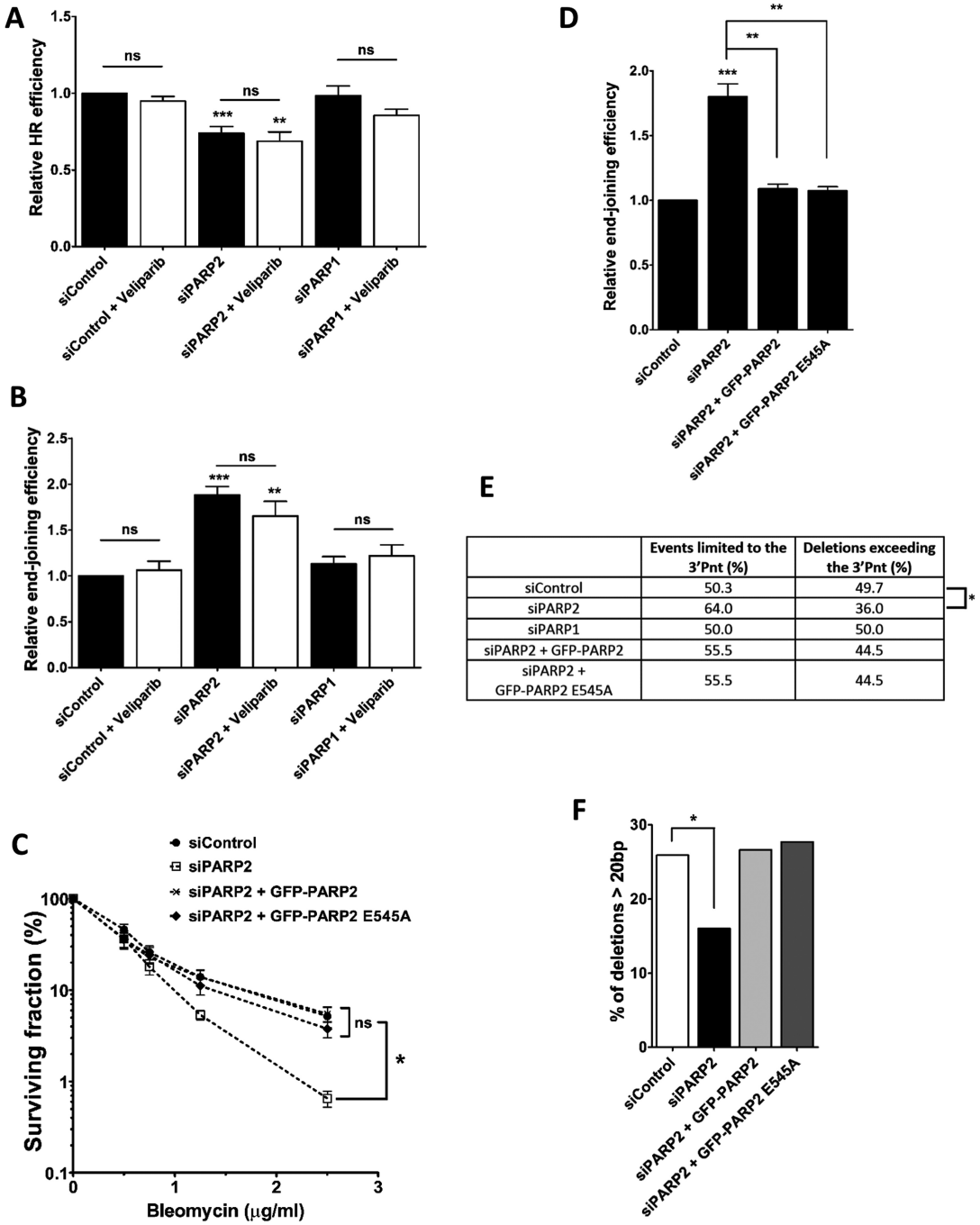

	Events limited to the 3′Pnt (%)	Deletions exceeding the 3′Pnt (%)
siControl	50.3	49.7
siPARP2	64.0	36.0
siPARP1	50.0	50.0
siPARP2 + GFP-PARP2	55.5	44.5
siPARP2 + GFP-PARP2 E545A	55.5	44.5

Figure 2. PARP2 promotes HR and A-EJ independently of its PARylation activity. HF DR-GFP cells (**A**) and HF EJ-CD4 cells (**B**) were transfected with the indicated siRNA for two days. When indicated, the PARP inhibitor Veliparib (10 μM) was added to the cell culture medium 1 h before transfection with the DsRed-I-SceI expression plasmid and kept until the relative repair efficiency was analysed. Data represent mean ± SEM from five experiments. $^{**}P < 0.01$; $^{***}P < 0.001$; ns, not significant. (**C**) Clonogenic cell survival was measured in HF EJ-CD4 cells transfected with the indicated siRNA and complemented with the wild type GFP-PARP2 or the PAR synthesis dead mutant GFP-PARP2 E545A. Cells in suspension were exposed to the indicated bleomycin concentration for 1 h before plating in drug-free media. Each treatment was repeated four times in triplicate. Data represents the mean ± SEM. $^{*}P < 0.05$; ns, not significant. (**D**) The EJ repair efficiency was measured in HF EJ-CD4 cells transfected with the indicated siRNA and complemented with the wild type GFP-PARP2 or the PARylation dead mutant GFP-PARP2 E545A. Data represent mean ± SEM from three experiments, $^{**}P < 0.01$; $^{***}P < 0.001$. (**E**) PARP2 depletion lowers the A-EJ repair efficiency. Analysis of the DNA sequence of repair junction from HF EJ-CD4 cells depleted for PARP1 or PARP2 and complemented or not with the wild type GFP-PARP2 or the PAR synthesis dead mutant GFP-PARP2 E545A. The EJ repair events are categorized according to the DNA sequence found at the repair junction. The events limited to the 3′Pnt are repair events for which the sequence at the repair junction includes at least one of the four nucleotides from the 3′Pnt generated by I-SceI cleavage; these events are dependent on the C-EJ pathway. The events with deletion exceeding the 3′Pnt, are events for which the sequence at the repair junction have four or more of the nucleotides at the I-SceI cleavage site that have been deleted; these events are dependent on the A-EJ pathway. Numbers indicate the percentage of junction events of either type and result from the analysis of 36–147 junction sequences per condition. (**F**) The graph represents the percentage of events with deletion of more than 20 base pairs at the repair junction. $^{*}P < 0.05$, statistics are presented only when differences are significant.

observed that the kinetics of EGFP-Ku80, EGFP-Ku70 and EGFP-XRCC4 recruitment at sites of laser-induced DNA damage is not altered in PARP2-depleted HeLa cells (Supplementary Figure S3A-D). Also, PARP2 and XRCC4 depletion had independent effects on EJ efficiency (Supplementary Figure S3E and F). Thus, we can exclude the possibility that PARP2 is regulating core C-EJ factors.

To gain more insight into the mechanism behind PARP2′s function during EJ, sequences at the EJ repair junctions in HF-EJ-CD4 cells were analyzed (Figure 2E and Supplementary Table S1). The EJ repair events were categorized into two classes according to the repair mechanism leading to the DNA sequence found at the repair junction (Supplementary Figure S1A and Supplementary Table S1). It was previously established that the repair of the I-Sce1 cleavage site by C-EJ was restricted to the four nucleotides of the 3′-protruding ends (3′-Pnt) generated by I-Sce1, whereas the repair of the I-Sce1 cleavage site by the non-conservative A-EJ involves deletions exceeding the four nucleotides of the 3′-Pnt (Supplementary Figure S1A and (20,57)). We found that the EJ repair events in the siControl or siPARP1 treated cells where evenly distributed between events involving 4 of the 3′-Pnt and deletions exceeding the 3′Pnt. This is consistent with PARP1′s role in the repair by A-EJ, only in the absence of functional Ku (41,58,59). In contrast, the frequency of events including the 3′Pnt reached 64% in PARP2 depleted cells (Figure 2E), indicating that PARP2 is promoting A-EJ. In addition, the frequency of repair events with deletions of more than 20 nucleotides beyond the 3′Pnt was decreased by 38% in PARP2 depleted cells compared to that of the control cells ($P = 0.0335$, Figure 2F). The expression of wild type PARP2 or PARP2 E545A restored both A-EJ frequencies and the deletion sizes to levels similar to that of control cells (Figure 2E-F).

These findings reveal a new function of PARP2 in modulating DSBR pathway choice that is independent of its PARylation activity. The observations that PARP2 does not affect the recruitment of core C-EJ factors but promotes HR, A-EJ and contributes to an increase in the deletion sizes at A-EJ junctions suggest a role of PARP2 in promoting resection during the repair of broken DNA-ends.

PARP2 stimulates DNA end-resection

The initiating step of DNA end-resection is shared between HR and A-EJ repair pathways and limitation or inhibition of the resection favors the DSB repair by the C-EJ pathway (1). PARP2 depletion reduces HR and A-EJ relative efficiency and decreases the size of the deletion at A-EJ repair junctions and also increases the usage of C-EJ. From these observations we hypothesised that PARP2 depletion could impede DNA end-resection. Resection at broken DNA ends is essential for RAD51 filament formation on ssDNA to drive strand exchange with a homologous template during HR. We thus quantified the formation of RAD51 foci detected by immunofluorescence after bleomycin treatment in U2OS cells. We found a strong reduction in RAD51 mobilization after bleomycin exposition in cells depleted for PARP2 ($P < 0.0001$) (Figure 3A-B). Exogenous expression of the wild type form or the PAR synthesis dead mutant of PARP2 fully restored RAD51 foci assembly in response to bleomycin in the siPARP2 treated U2OS cells (Figure 3A and Supplementary Figure S3G). These results suggest that PARP2 stimulate HR independently of its PAR synthesis actvity.

We also quantified by flow cytometry the accumulation of the single strand DNA binding complex RPA at the chromatin of bleomycin treated cells. We observed that the absence of PARP2 impedes the induction of the RPA signal at the chromatin after bleomycin treatment in U2OS cells ($P = 0.0047$, 6 h post bleomycin treatment, Figure 3C and D) and HeLa cells ($P = 0.0073$, Supplementary Figure S3H). PARP2 depletion also led to a strong reduction of the frequency of bleomycin-induced RPA foci detected by immunofluorescence in U2OS cells ($P = 0.001$, Supplementary Figure S3I). To directly assess the presence of single-stranded DNA in response to bleomycin exposure, we analysed BrdU signals by immunofluorescence without DNA denaturation. The depletion of PARP2 in U2OS cells significantly diminished the formation BrdU foci induced by bleomycin treatment (Figure 3E and F). The observations that PARP2-deficiency results in a significant reduction in the formation of Rad51 foci, RPA accumulation at the chromatin and BrdU foci detection after bleomycin treatment indicates that PARP2 favors broken DNA end-resection.

PARP2 stimulates DNA end-resection by preventing 53BP1 accumulation

The resection barrier established by 53BP1 and its effector RIF1 favor C-EJ and impedes the HR, SSA and A-EJ pathways (5,6,8–11). Based on our results we speculated that PARP2 might alleviate the end-resection barrier sustained by 53BP1. To test this we analysed 53BP1 foci assembly in response to bleomycin in U2OS cells. PARP2 depletion greatly increased the average number of bleomycin-induced 53BP1 foci in U2OS cells nuclei ($P < 0.001$, Figure 4A and B). The increase in number of bleomycin-induced 53BP1 foci in siPARP2 treated U2OS cells was suppressed by the reintroduction of either the wild type PARP2 or PARP2 E545A mutant ($P < 0.001$ and $P < 0.001$, respectively) (Figure 4A and B). We next monitored the dynamics of GFP-53BP1 recruitment at sites of DNA damage induced by laser-microirradiation. We observed a significant higher enrichment of the GFP-53BP1 protein at laser-induced DNA damage sites in PARP2-depleted cells, as early as 2 minutes post-irradiation ($P < 0.001$, Figure 4C and D), whilst the depletion of 53BP1 had no effect on the dynamics of GFP-PARP2 recruitment at sites of DNA damage (Supplementary Figure S4G). These results demonstrate that PARP2 limits the 53BP1 accumulation at sites of DNA damage independently of its PAR synthesis activity.

We next investigated the effect of 53BP1 silencing in PARP2-depleted cells on the repair efficiency of I-Sce1 cleaved sites. We found that the double depletion of 53BP1 and PARP2 (Figure 4I) suppresses the defect in HR (Figure 4E), SSA (Figure 4F) in the U2OS SA-GFP cells ((19) and Supplementary Figure S4A) and A-EJ (Figure 4G and H) of PARP2 depleted cells. In addition, the silencing of 53BP1 in the PARP2 depleted cells restores the C-EJ efficiency back to the levels seen in siRNA control cells (Fig-

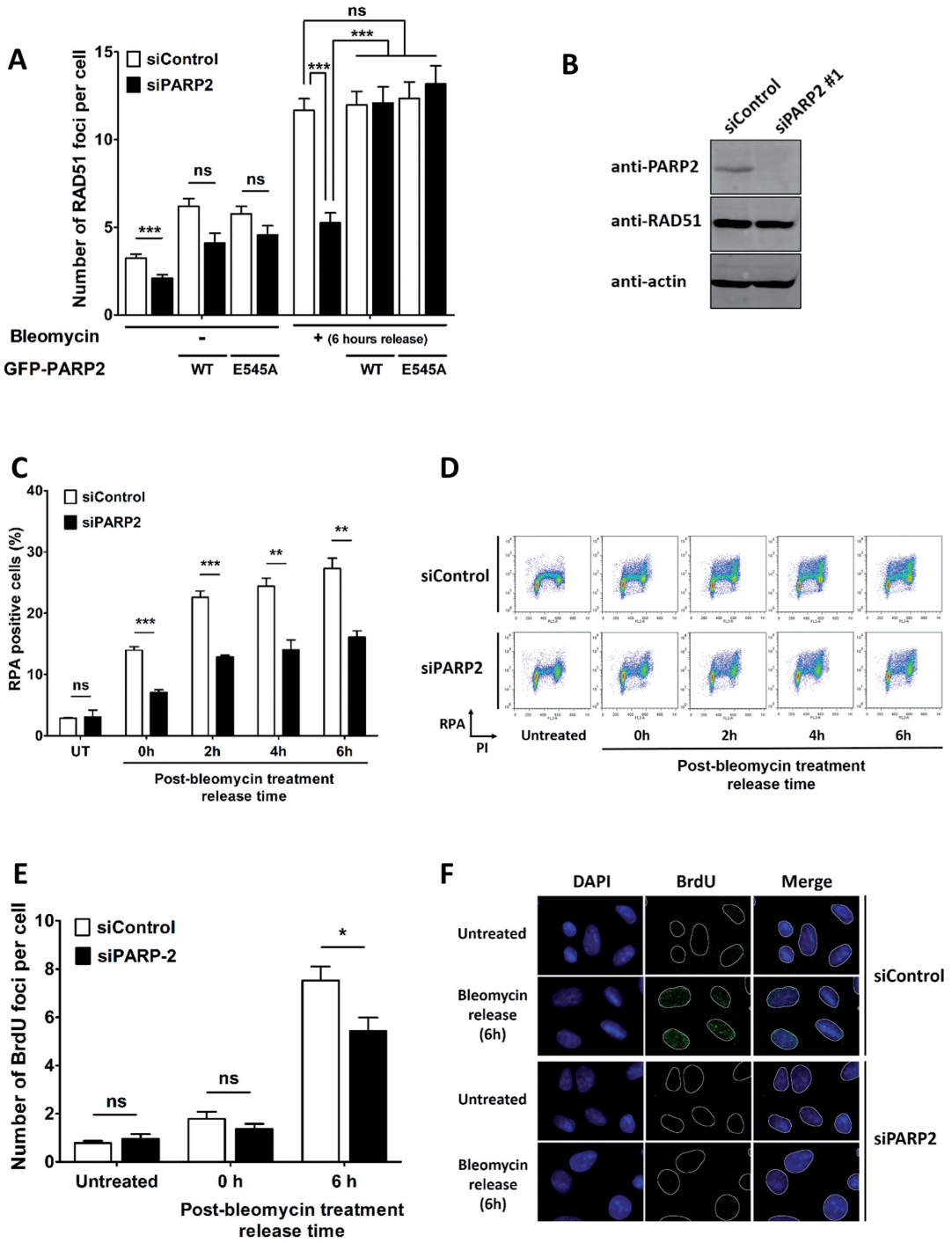

Figure 3. PARP2 stimulates DNA end-resection. (**A**) Cell transfected for 48 h with the indicated siRNA were then complemented with the wild type GFP-PARP2 or the PAR synthesis dead mutant GFP-PARP2 E545A and treated or not for 2 h with 25 μg/ml bleomycin and released into drug-free medium for 6 h (6 hours release). The cells were fixed and stained for the immunodetection of RAD51. Data represent mean number of foci per nuclei ± 95% CI from at least 850 cells analysed from three independent experiments. ***$P < 0.001$ (one-way ANOVA test). (**B**) Western blot analysis of whole cell extracts from U2OS cells transfected with the indicated siRNA. (**C**) The proportion of U2OS cells positive for RPA32 subunit signal is presented in siControl and siPARP2 transfected cells. Cell transfected for 48 h with the indicated siRNA were untreated (UT) or treated for 2 h with 25 μg/ml bleomycin and then released in fresh medium for the indicated time points (0 h, indicates no release). The soluble proteins were extracted and the cells were stained for the immunodetection of the RPA32 subunit and analysed by flow cytometry. *$P < 0.05$; **$P < 0.01$; ***$P < 0.001$; ns, not significant. (**D**) Representative flow cytometry dot plot graphs showing the U2OS cell population treated as indicated and stained with propidium iodide (PI) and for RPA32 (RPA). (**E**) Analysis of the number of BrdU foci in siControl and siPARP2 transfected U2OS cells. Cells were transfected with the indicated siRNA for 48 h were treated or not for 2 h with 25 μg/ml bleomycin and released into drug-free medium for 6 h (bleomycin release time, 6 h). Cells were then processed for BrdU immunofluorescence without DNA denaturation at the indicated time post-release. Data represent mean number of foci per nuclei ± 95% CI from a total of at least 850 cells analysed from three independent experiments. *$P < 0.05$; ns, not significant (one-way ANOVA test). (**F**) Representative images of U2OS cells fixed on coverslips and BrdU immunostained for foci quantification presented in (E).

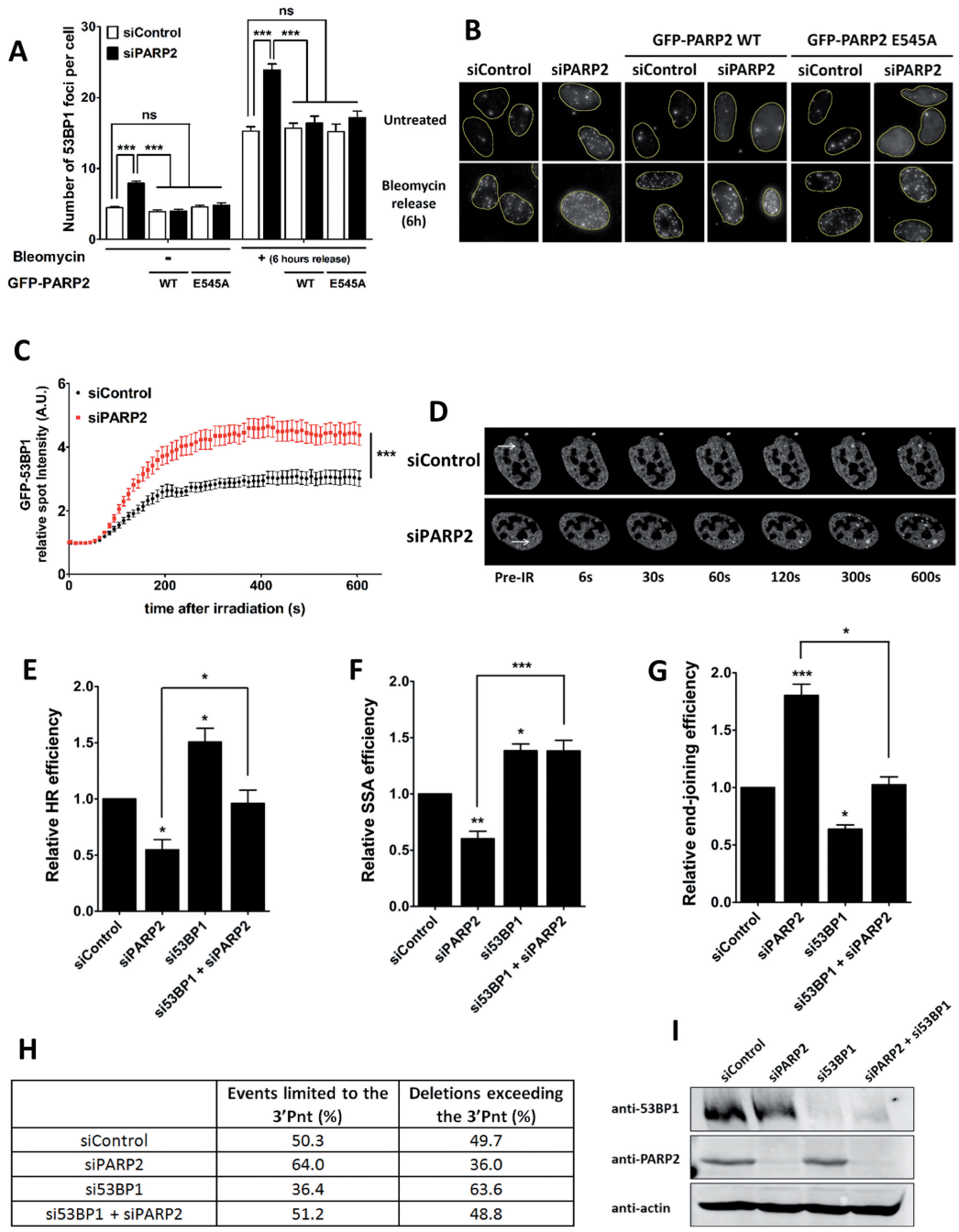

	Events limited to the 3'Pnt (%)	Deletions exceeding the 3'Pnt (%)
siControl	50.3	49.7
siPARP2	64.0	36.0
si53BP1	36.4	63.6
si53BP1 + siPARP2	51.2	48.8

Figure 4. PARP2 stimulates DNA end-resection by preventing 53BP1 accumulation at broken DNA ends. (**A**) U2OS cells were transfected for 48 h with the indicated siRNA and when indicated the siRNA transfected cells were complemented with the wild type GFP-PARP2 or the PAR synthesis dead mutant GFP-PARP2 E545A. The cells were treated or not for 2 h with 25 μg/ml bleomycin and were released into drug-free medium for 6 h (6 h release). The cells were fixed and stained for the immunodetection of 53BP1. Data represent the mean number of foci per nuclei ± 95% CI from at least 1200 cells analysed from three independent experiments. ***$P < 0.001$ (one-way ANOVA test). (**B**) Representative images of U2OS cells fixed on coverslips, and 53BP1 immunostained for foci quantification presented in (A). (**C**) HeLa cells were transfected with siControl or siPARP2 for 48 h and were subsequently transected for 24 h with GFP-53BP1 fusion protein expression plasmid. For the recruitment analysis, 10 μg/ml Hoechst 33258 was added to the culture medium 5 min before induction of DNA damage by micro-irradiation with a two-photon laser (810 nm). The irradiated cells were imaged every 10 s for 10 min. Data represents mean relative spot intensity ± SEM, n = 25–28 individual cells from a minimum of five independent experiments. (**D**) Representative images of the recruitment of the GFP-53BP1 fluorescent-tagged protein. (**E**) The relative repair efficiency by HR is determined in HF DR-GFP cells transfected with the indicated siRNA. Data represent mean ± SEM from four experiments. * $P < 0.05$, statistics are presented only when differences are significant. (**F**) The relative repair efficiency by SSA is determined in U2OS SA-GFP cells transfected with the indicated siRNA. Data represent mean ± SEM from three experiments. *$P < 0.05$; **$P < 0.01$; ***$P < 0.001$. (**G**) The relative repair efficiency by EJ was measured in HF EJ-CD4 cells transfected with the indicated siRNA. Data represent mean ± SEM from at least three experiments. *$P < 0.05$; ***$P < 0.001$, statistics are presented only when differences are significant. (**H**) Analysis of the DNA sequence of repair junction from HF EJ-CD4 cells transfected with the indicated siRNA. Data represent the percentage of repair events of each class and result from the analysis of 41–147 junction sequences per condition. (**I**) Analysis of proteins expression by western blot of cell extracts from HF EJ-CD4 cells from (G) and (H).

ure 4H). Importantly, depleting PARP2 has no effect on the protein levels of 53BP1 (Figure 4I). Silencing of the 53BP1 co-factor, RIF1, also partially rescued HR and EJ efficiency defect in cells depleted for PARP2 (Supplementary Figure S4B–D).

Collectively, our data clearly indicate that PARP2 is contributing to the DSBR pathway choice by limiting 53BP1 accumulation at sites of DNA damage, thus allowing broken DNA-ends resection dependent repair pathways in disfavor of the C-EJ.

PARP2 co-operates with BRCA1 to stimulate CtIP-dependent end-resection

The resection step is initiated by the activity of the CtIP protein (60). The action of CtIP is antagonized by the end-resection barrier sustained by 53BP1 and its partners (61). We speculated that the PARP2 protein might control CtIP-dependent end-resection by limiting 53BP1 accumulation at broken-DNA ends. To investigate the relationship between PARP2 and CtIP proteins during DSBR, we down-regulated PARP2 and CtIP expression in HF DR-GFP, U2OS SA-GFP and HF EJ-CD4 cells. CtIP depletion (Figure 5A) led to a significant decrease in the relative efficiency of HR (Figure 5C), SSA (Figure 5D) and A-EJ (Figure 5E-F) pathways which all depend on the initiation of broken DNA-ends resection. Conversely, CtIP depletion (Figure 5A) significantly increased the relative C-EJ efficiency (Figure 5E and F). In addition, depleting PARP2 in the CtIP depleted cells did not affect the repair efficiency in CtIP depleted cells. These observations are in agreement with the well-established function of CtIP in initiating ssDNA formation at broken DNA-ends during homology-dependent repair (12,13,62), and indicate that the function of PARP2 in promoting end-resection is dependent on CtIP.

It has been described that BRCA1 alleviates the barrier sustained by the 53BP1 pathway, allowing CtIP-dependent DNA end-resection (63–65) and that the removal of 53BP1 in BRCA1 mutant cells is sufficient to allow CtIP-dependent DNA end-resection, which partially restores HR and SSA efficiency (5,8–10,61,66). Considering our data show that PARP2 is contributing to the DSBR pathways choice by limiting 53BP1 accumulation at sites of DNA damage, we investigated whether PARP2 and BRCA1 cooperate in promoting HR, SSA and A-EJ and in suppressing C-EJ. The silencing of BRCA1 (Figure 5B) reduced HR (Figure 5C), SSA (Figure 5D) and A-EJ (Figure 5F) efficiency, this is similar to the effect of CtIP or PARP2 depletion on these repair pathways. The depletion of PARP2 in BRCA1 depleted cells (Figure 5B) did not further reduce HR (Figure 5C), SSA (Figure 5D) and A-EJ (Figure 5F) efficiency, indicating that both proteins function together for the repair of I-Sce1 induced-cut by these resection-dependent pathways.

BRCA1 not only promotes end-resection dependent DSBR, it is also required for the efficient repair of I-Sce1 induced-cut by EJ (67–70). We confirmed that BRCA1 depletion significantly reduces the EJ efficiency (Figure 5E). In addition, the EJ efficiency in cells depleted of PARP2 or 53BP1 is further decreased when BRCA1 is also depleted in these cells (Figure 5E and Supplementary Figure S5), suggesting that BRCA1 is promoting both A-EJ and C-EJ. These results indicate that the role for BRCA1 in promoting C-EJ is distinct from the role of PARP2 which suppresses C-EJ by limiting 53BP1 accumulation at DNA damage sites (Figure 4). Our observations are in agreement with the previously identified role for BRCA1 in promoting C-EJ independently of 53BP1 (68).

To further characterize the genetic interactions between PARP2 and BRCA1 during DNA repair, we analysed the importance of these proteins in promoting cell viability in response to bleomycin. The depletion of either PARP2 or BRCA1 increased HeLa cells sensitivity to bleomycin, whereas the relatively high sensitivity of BRCA1-depleted HeLa cells to bleomycin did not further increase when PARP2 was depleted (Figure 5G-H). Taken together, these observations indicate that PARP2 and BRCA1 contribute together to DSBR by the HR, SSA and A-EJ pathway, and also confirm that the role for BRCA1 in C-EJ is independent of 53BP1.

DISCUSSION

In this study, we describe a new function for the PARP2 protein in controlling DSBR pathway choice. Indeed, we show that PARP2 prevents the accumulation of 53BP1 at damaged chromatin and allows CtIP-dependent broken DNA end-resection. Therefore, we propose a model in which PARP2 is limiting the accumulation of the resection barrier imposed by 53BP1 at broken DNA ends, which in turn together with BRCA1 favors the channeling of DSB repair towards resection dependent repair pathways (HR, SSA and A-EJ) rather than C-EJ (Figure 6).

We also reported that C-EJ inhibition and HR promotion by PARP2 were independent on its PARylation activity. Previously known PARP2 functions in DNA repair, such as preventing illegitimate IgH/c-myc translocations during class switch recombination (CSR) in mice (46), or promoting the restart of stalled replication forks by HR (35), were associated with its PARylation activity. The PARP2 function we report here, that does not require PARylation activity, is clearly new and distinct from the previously known PARP2 functions in DSBR.

Our observations that neither PARP1, nor PARP's catalytic activity, regulate DSBR efficiency is consistent with PARP1′s role in the choice of A-EJ only in the absence of functional Ku (41,58,59). Nonetheless, it does not preclude a potential role of PARP1 and its catalytic activity for DSBR in a more complex chromatin context. Indeed, PARP1 is important for the recruitment of several chromatin remodelers, which in turn stimulate the recruitment of DNA repair factors at the damaged chromatin (71–73).

53BP1 is acting as a barrier to resection of the broken DNA ends, blocking CtIP/MRN-dependent ends processing (18,74). However, the end-resection defect or the genomic instability in a CtIP deficient context is not reverted by 53BP1 loss, showing that the displacement of 53BP1 and its partners is required for CtIP-dependent end-resection (61). Likewise, our results highlight that the functions of PARP2 in stimulating HR, SSA and A-EJ are dependent on the expression of CtIP, showing that PARP2 and CtIP present an epistatic interaction in promoting these path-

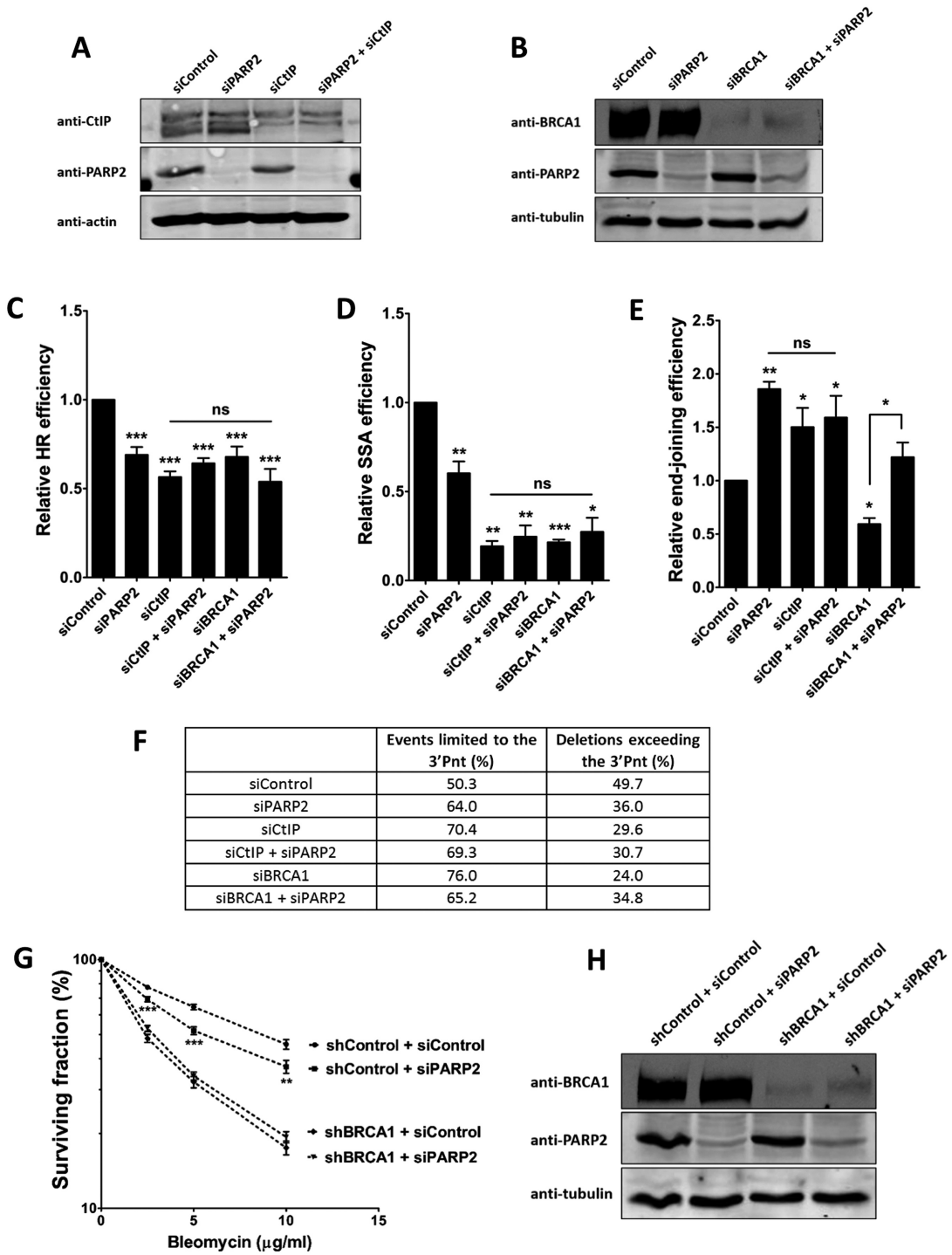

	Events limited to the 3'Pnt (%)	Deletions exceeding the 3'Pnt (%)
siControl	50.3	49.7
siPARP2	64.0	36.0
siCtIP	70.4	29.6
siCtIP + siPARP2	69.3	30.7
siBRCA1	76.0	24.0
siBRCA1 + siPARP2	65.2	34.8

Figure 5. CtIP is required for PARP2 to stimulate DNA end-resection. Analysis of (**A**) CtIP or (**B**) BRCA1 protein expression by western blot of whole cell extracts prepared from HF EJ-CD4 cells transfected with the indicated siRNA. Protein extracts prepared 48 h after transfection with the indicated siRNA. The relative repair efficiency of I-SceI-induced double strand ends by (**C**) HR in HF DR-GFP cells or by (**D**) SSA in U2OS cells carrying the SA-GFP substrate was determined. Values are mean ± SEM from at least four (HF DR-GFP) and least three (U2OS SA-GFP) independent experiments. $*P < 0.05$; $**P < 0.01$; $***P < 0.001$; ns, not significant. (**E**) The relative repair efficiency of I-SceI-induced double strand ends by EJ in the HF EJ-CD4 cells transfected with the indicated siRNA was determined. Data represent mean ± SEM from at least three experiments. $*P < 0.05$; $**P < 0.01$; ns, not significant. (**F**) Analysis of the DNA sequence of repair junction from HF EJ-CD4 cells transfected with the indicated siRNA. Data represent the percentage of repair events of each classes of EJ events and result from the analysis of 26–147 junction sequences per condition. (**G**) Effect of PARP2 and/or BRCA1 depletion on bleomycin induced HeLa cells cytotoxicity assessed using a clonogenic surviving assay. The HeLa shControl and HeLa shBRCA1 were transfected with the indicated siRNA for 48 h. Cells in suspension were exposed to the indicated bleomycin concentration for 1 h before plating. Each data point represents mean ± SEM of six independent experiments with each dose in triplicate. $**P < 0.01$; $***P < 0.001$, statistics are presented only when differences are significant (Mann-Whitney test). (**I**) Representative immunoblot showing the levels of the indicated proteins HeLa cells 48 h post transfection with the indicated siRNA.

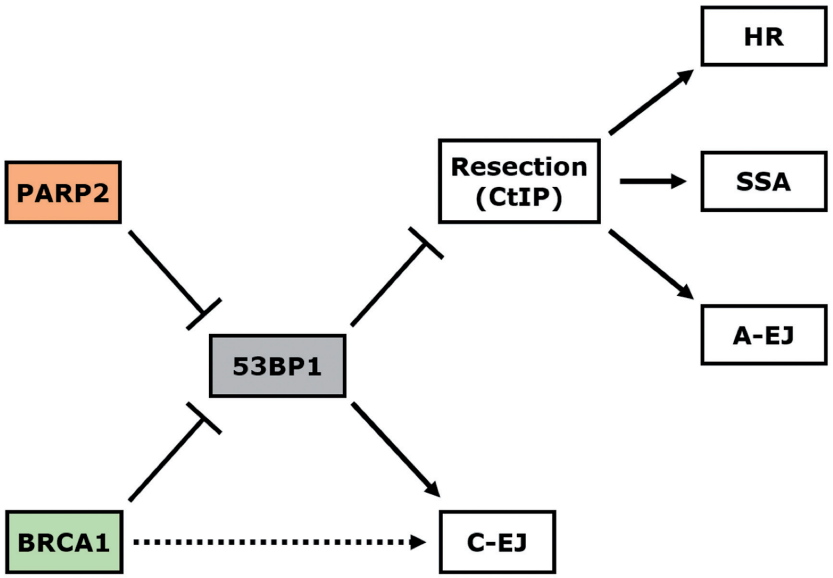

Figure 6. Model for the role of PARP2 in the DSBR pathway choice.

ways, which in turn repress C-EJ. In addition, considering that both the increase in the relative C-EJ efficiency and the decrease in HR observed when PARP2 is absent are fully reverted when the resection barrier imposed by 53BP1 is removed, further suggests that PARP2 does not directly stimulate the catalytic reaction of end-resection. Instead, we propose that PARP2 limits the accumulation of 53BP1 at broken DNA ends in favor of CtIP/MRN-dependent end-resection, thereby placing PARP2 upstream of CtIP/MRN DNA end-processing functions.

How PARP2 is regulating the recruitment of 53BP1 remains to be fully understood. To date, the initial recruitment of 53BP1 to DNA damage sites has been shown to be modulated by several mechanisms. First, 53BP1 recruitment is dependent on H2AK15 ubiquitylation by the RNF8 and RNF168 ubiquitin ligases in response to DNA damage (75). Second, the displacement of the TIRR protein from 53BP1′s tudor domains and the degradation of the JMJD2A and L3MBTL1 proteins allows 53BP1 binding to H4K20me2 (76–79). Third, the BLM helicase has been shown to stimulate the assembly of 53BP1 foci after gamma irradiation (11). It has been reported that up-regulation of the RNF168 pathway is sufficient to compensate for the defect in 53BP1 foci formation caused by the low abundance of ubiquitin in cells treated with the proteasome inhibitor MG-132 (80). We found that 53BP1 foci formation were prevented in PARP2 depleted cells treated with the MG-132 (Supplementary Figure S4E-F), suggesting that PARP2 is not acting through the downregulation of RNF8-RNF168 pathway. PARP2 protein has a strong affinity for phosphorylated broken DNA-ends (40,54), and we also observed that the *in vivo* affinity of PARP2 for RIF1 was not affected by bleomycin treatment (Supplementary Figure S4H) but found no evidence for direct PARP2 and 53BP1 interactions (data not shown). We cannot however exclude the possibility that PARP2 could suppress the role of the RIF1 protein partner TIRR in the unmasking of 53BP1′s tudor domains (81), thereby regulating indirectly 53BP1′s recognition of H4K20me2.

We also found that the protective function of PARP2 against the genotoxic effect of bleomycin, a radiomimetic drug that directly induces SSBs and DSBs (with a 6:1 ratio) (51), depends on PARP2 protein expression and not on its PARylation activity. In S-phase, the progression of replication fork through unrepaired SSBs can also result in DSB. The requirement of PARP2 for the efficient formation of ssDNA, and the formation of HR foci in response to bleomycin, are consistent with the role for the PARP2 protein in regulating the accumulation of 53BP1 at broken DNA ends. However, PARP2 depletion did not further sensitize BRCA1 deficient cells to bleomycin despite its role in SSBs resolution (34), suggesting that PARP2, in cooperation with BRCA1, promotes cells survival.

Several studies have shown that BRCA1 is involved in the regulation of end-resection initiation by displacing 53BP1 and its partners from DSBs (63–65). Our results suggest that PARP2 and BRCA1 play similar roles in alleviating 53BP1-dependent barrier, thus facilitating the CtIP-dependent DNA end-resection essential for HR and SSA to proceed.

In addition, we confirmed that BRCA1 and 53BP1 have distinct functions in stimulating EJ (this work and (68)). The observation that the absence of both BRCA1 and PARP2 restores EJ relative efficiency mostly through C-EJ, indicate that BRCA1 and PARP2 are not redundant during C-EJ. We speculate that the multiple functions of BRCA1, which include the removal of the Ku complex (68–70) as well as promoting limited end resection activities (67), are required to support both C-EJ and A-EJ.

In conclusion, our findings identify a new crucial role for the PARP2 protein in regulating DSBR pathway choice, independently of its PARylation activity. PARP2 is limiting 53BP1 accumulation onto broken DNA, facilitating the CtIP-dependent DNA end-resection and thereby limiting

the repair of double strand breaks by C-EJ. Moreover, our study reveals an independent function of BRCA1 in EJ that is yet to be elucidated. Further studies to decipher the PARylation activity-dependent and -independent functions of PARP2 during DSBR will be of prime importance in the context where small molecule inhibiting PAR synthesis appear likely to become a fundamental component in the management of patients with BRCA mutation associated tumors.

SUPPLEMENTARY DATA

Supplementary Data are available at NAR online.

ACKNOWLEDGEMENTS

We thank Marie-Noëlle Soler for the measurements of the Power output of bi-photon laser for induced photodamage. *Authors contribution*: The authors have made the following declarations about their contributions; Conceived and designed the experiments: V.P., A.F. Performed the experiments: A.F., V.P. Analyzed the data: A.F., V.P. Contributed reagents/materials/analysis tools: J.G.B., B.L., J.H., M.A.G. Wrote the paper: A.F., V.P., J.G.B., B.L., J.H., M.A.G.

FUNDING

PICT-IBiSA@Orsay Imaging Facility of the Institut Curie supported by the French National Research Agency through the 'Investissment for the future' program (France-BioImaging) [ANR-10-INSB-04]; 'Fondation-EDF' [RB2013-18, RB2014-09 to V.P.]; Ligue Nationale Contre le Cancer (comité de l'Essonne); INSERM [V.P. is an INSERM research scientist in UMR3348]; CNRS and the Institut Curie; Ministère de l'Enseignement supérieur, de la Recherche et de l'Innovation and the 'Fondation ARC pour la recherche sur le cancer' are acknowledged for a PhD grant (to A.F.).
Conflict of interest statement. None declared.

REFERENCES

1. Ceccaldi,R., Rondinelli,B. and D'Andrea,A.D. (2016) Repair pathway choices and consequences at the double-strand break. *Trends Cell Biol.*, **26**, 52–64.
2. Sun,J., Lee,K.J., Davis,A.J. and Chen,D.J. (2012) Human Ku70/80 protein blocks exonuclease 1-mediated DNA resection in the presence of human Mre11 or Mre11/Rad50 protein complex. *J. Biol. Chem.*, **287**, 4936–4945.
3. Shim,E.Y., Chung,W.H., Nicolette,M.L., Zhang,Y., Davis,M., Zhu,Z., Paull,T.T., Ira,G. and Lee,S.E. (2010) Saccharomyces cerevisiae Mre11/Rad50/Xrs2 and Ku proteins regulate association of Exo1 and Dna2 with DNA breaks. *EMBO J.*, **29**, 3370–3380.
4. Boersma,V., Moatti,N., Segura-Bayona,S., Peuscher,M.H., van der Torre,J., Wevers,B.A., Orthwein,A., Durocher,D. and Jacobs,J.J. (2015) MAD2L2 controls DNA repair at telomeres and DNA breaks by inhibiting 5' end resection. *Nature*, **521**, 537–540.
5. Escribano-Diaz,C., Orthwein,A., Fradet-Turcotte,A., Xing,M., Young,J.T., Tkac,J., Cook,M.A., Rosebrock,A.P., Munro,M., Canny,M.D. *et al.* (2013) A cell cycle-dependent regulatory circuit composed of 53BP1-RIF1 and BRCA1-CtIP controls DNA repair pathway choice. *Mol. Cell*, **49**, 872–883.
6. Feng,L., Fong,K.W., Wang,J., Wang,W. and Chen,J. (2013) RIF1 counteracts BRCA1-mediated end resection during DNA repair. *J. Biol. Chem.*, **288**, 11135–11143.
7. Wang,J., Aroumougame,A., Lobrich,M., Li,Y., Chen,D., Chen,J. and Gong,Z. (2014) PTIP associates with Artemis to dictate DNA repair pathway choice. *Genes Dev.*, **28**, 2693–2698.
8. Zimmermann,M., Lottersberger,F., Buonomo,S.B., Sfeir,A. and de Lange,T. (2013) 53BP1 regulates DSB repair using Rif1 to control 5' end resection. *Science*, **339**, 700–704.
9. Chapman,J.R., Barral,P., Vannier,J.-B., Borel,V., Steger,M., Tomas-Loba,A., Sartori,Alessandro A., Adams,Ian R., Batista,Facundo D. and Boulton,Simon J. (2013) RIF1 is essential for 53BP1-dependent nonhomologous end joining and suppression of DNA double-strand break resection. *Mol. Cell*, **49**, 858–871.
10. Bunting,S.F., Callén,E., Wong,N., Chen,H.-T., Polato,F., Gunn,A., Bothmer,A., Feldhahn,N., Fernandez-Capetillo,O., Cao,L. *et al.* (2010) 53BP1 inhibits homologous recombination in Brca1-deficient cells by blocking resection of DNA breaks. *Cell*, **141**, 243–254.
11. Grabarz,A., Guirouilh-Barbat,J., Barascu,A., Pennarun,G., Genet,D., Rass,E., Germann,S.M., Bertrand,P., Hickson,I.D. and Lopez,B.S. (2013) A role for BLM in double-strand break repair pathway choice: prevention of CtIP/Mre11-mediated alternative nonhomologous end-joining. *Cell Rep.*, **5**, 21–28.
12. Bennardo,N., Cheng,A., Huang,N. and Stark,J.M. (2008) Alternative-NHEJ is a mechanistically distinct pathway of mammalian chromosome break repair. *PLos Genet.*, **4**, e1000110.
13. Rass,E., Grabarz,A., Plo,I., Gautier,J., Bertrand,P. and Lopez,B.S. (2009) Role of Mre11 in chromosomal nonhomologous end joining in mammalian cells. *Nat. Struct. Mol. Biol.*, **16**, 819–824.
14. Xie,A., Kwok,A. and Scully,R. (2009) Role of mammalian Mre11 in classical and alternative nonhomologous end joining. *Nat. Struct. Mol. Biol.*, **16**, 814–818.
15. Deriano,L., Stracker,T.H., Baker,A., Petrini,J.H. and Roth,D.B. (2009) Roles for NBS1 in alternative nonhomologous end-joining of V(D)J recombination intermediates. *Mol. Cell*, **34**, 13–25.
16. Wang,H., Perrault,A.R., Takeda,Y., Qin,W., Wang,H. and Iliakis,G. (2003) Biochemical evidence for Ku-independent backup pathways of NHEJ. *Nucleic Acids Res.*, **31**, 5377–5388.
17. Kabotyanski,E.B., Gomelsky,L., Han,J.-O., Roth,D.B. and Stamato,T.D. (1998) Double-strand break repair in Ku86- and XRCC4-deficient cells. *Nucleic Acids Res.*, **26**, 5333–5342.
18. Guirouilh-Barbat,J., Gelot,C., Xie,A., Dardillac,E., Scully,R. and Lopez,B.S. (2016) 53BP1 protects against CtIP-dependent capture of ectopic chromosomal sequences at the junction of distant double-strand breaks. *PLos Genet.*, **12**, e1006230.
19. Stark,J.M., Pierce,A.J., Oh,J., Pastink,A. and Jasin,M. (2004) Genetic steps of mammalian homologous repair with distinct mutagenic consequences. *Mol. Cell. Biol.*, **24**, 9305–9316.
20. Guirouilh-Barbat,J., Rass,E., Plo,I., Bertrand,P. and Lopez,B.S. (2007) Defects in XRCC4 and KU80 differentially affect the joining of distal nonhomologous ends. *Proc. Natl. Acad. Sci. U.S.A.*, **104**, 20902–20907.
21. Chiruvella,K.K., Liang,Z. and Wilson,T.E. (2013) Repair of double-strand breaks by end joining. *Cold Spring Harbor Perspect. Biol.*, **5**, a012757.
22. Nimonkar,A.V., Genschel,J., Kinoshita,E., Polaczek,P., Campbell,J.L., Wyman,C., Modrich,P. and Kowalczykowski,S.C. (2011) BLM-DNA2-RPA-MRN and EXO1-BLM-RPA-MRN constitute two DNA end resection machineries for human DNA break repair. *Genes Dev.*, **25**, 350–362.
23. Gravel,S., Chapman,J.R., Magill,C. and Jackson,S.P. (2008) DNA helicases Sgs1 and BLM promote DNA double-strand break resection. *Genes Dev.*, **22**, 2767–2772.
24. Karanja,K.K., Cox,S.W., Duxin,J.P., Stewart,S.A. and Campbell,J.L. (2012) DNA2 and EXO1 in replication-coupled, homology-directed repair and in the interplay between HDR and the FA/BRCA network. *Cell Cycle*, **11**, 3983–3996.
25. Fukushima,T., Takata,M., Morrison,C., Araki,R., Fujimori,A., Abe,M., Tatsumi,K., Jasin,M., Dhar,P.K., Sonoda,E. *et al.* (2001) Genetic analysis of the DNA-dependent protein kinase reveals an inhibitory role of Ku in late S-G2 phase DNA double-strand break repair. *J. Biol. Chem.*, **276**, 44413–44418.
26. Pierce,A.J., Hu,P., Han,M., Ellis,N. and Jasin,M. (2001) Ku DNA end-binding protein modulates homologous repair of double-strand breaks in mammalian cells. *Genes Dev.*, **15**, 3237–3242.
27. Li,X. and Heyer,W.-D. (2008) Homologous recombination in DNA repair and DNA damage tolerance. *Cell Res.*, **18**, 99–113.

28. Mansour,W.Y., Schumacher,S., Rosskopf,R., Rhein,T., Schmidt-Petersen,F., Gatzemeier,F., Haag,F., Borgmann,K., Willers,H. and Dahm-Daphi,J. (2008) Hierarchy of nonhomologous end-joining, single-strand annealing and gene conversion at site-directed DNA double-strand breaks. *Nucleic Acids Res.*, **36**, 4088–4098.
29. Ame,J.C., Rolli,V., Schreiber,V., Niedergang,C., Apiou,F., Decker,P., Muller,S., Hoger,T., Menissier-de Murcia,J. and de Murcia,G. (1999) PARP-2, A novel mammalian DNA damage-dependent poly(ADP-ribose) polymerase. *J. Biol. Chem.*, **274**, 17860–17868.
30. Rulten,S.L., Fisher,A.E., Robert,I., Zuma,M.C., Rouleau,M., Ju,L., Poirier,G., Reina-San-Martin,B. and Caldecott,K.W. (2011) PARP-3 and APLF function together to accelerate nonhomologous end-joining. *Mol. Cell*, **41**, 33–45.
31. Boehler,C., Gauthier,L.R., Mortusewicz,O., Biard,D.S., Saliou,J.-M., Bresson,A., Sanglier-Cianferani,S., Smith,S., Schreiber,V., Boussin,F. *et al.* (2011) Poly(ADP-ribose) polymerase 3 (PARP3), a newcomer in cellular response to DNA damage and mitotic progression. *Proc. Natl. Acad. Sci. U.S.A.*, **108**, 2783–2788.
32. Wahlberg,E., Karlberg,T., Kouznetsova,E., Markova,N., Macchiarulo,A., Thorsell,A.G., Pol,E., Frostell,A., Ekblad,T., Oncu,D. *et al.* (2012) Family-wide chemical profiling and structural analysis of PARP and tankyrase inhibitors. *Nat. Biotechnol.*, **30**, 283–288.
33. Menissier de Murcia,J., Ricoul,M., Tartier,L., Niedergang,C., Huber,A., Dantzer,F., Schreiber,V., Ame,J.C., Dierich,A., LeMeur,M. *et al.* (2003) Functional interaction between PARP-1 and PARP-2 in chromosome stability and embryonic development in mouse. *EMBO J.*, **22**, 2255–2263.
34. Schreiber,V., Ame,J.C., Dolle,P., Schultz,I., Rinaldi,B., Fraulob,V., Menissier-de Murcia,J. and de Murcia,G. (2002) Poly(ADP-ribose) polymerase-2 (PARP-2) is required for efficient base excision DNA repair in association with PARP-1 and XRCC1. *J. Biol. Chem.*, **277**, 23028–23036.
35. Bryant,H.E., Petermann,E., Schultz,N., Jemth,A.S., Loseva,O., Issaeva,N., Johansson,F., Fernandez,S., McGlynn,P. and Helleday,T. (2009) PARP is activated at stalled forks to mediate Mre11-dependent replication restart and recombination. *EMBO J.*, **28**, 2601–2615.
36. Navarro,J., Gozalbo-Lopez,B., Mendez,A.C., Dantzer,F., Schreiber,V., Martinez,C., Arana,D.M., Farres,J., Revilla-Nuin,B., Bueno,M.F. *et al.* (2017) PARP-1/PARP-2 double deficiency in mouse T cells results in faulty immune responses and T lymphomas. *Sci. Rep.*, **7**, 41962.
37. Langelier,M.F., Riccio,A.A. and Pascal,J.M. (2014) PARP-2 and PARP-3 are selectively activated by 5' phosphorylated DNA breaks through an allosteric regulatory mechanism shared with PARP-1. *Nucleic Acids Res.*, **42**, 7762–7775.
38. Obaji,E., Haikarainen,T. and Lehtio,L. (2016) Characterization of the DNA dependent activation of human ARTD2/PARP2. *Sci. Rep.*, **6**, 34487.
39. Sukhanova,M.V., Abrakhi,S., Joshi,V., Pastre,D., Kutuzov,M.M., Anarbaev,R.O., Curmi,P.A., Hamon,L. and Lavrik,O.I. (2016) Single molecule detection of PARP1 and PARP2 interaction with DNA strand breaks and their poly(ADP-ribosyl)ation using high-resolution AFM imaging. *Nucleic Acids Res.*, **44**, e60.
40. Kutuzov,M.M., Khodyreva,S.N., Ame,J.C., Ilina,E.S., Sukhanova,M.V., Schreiber,V. and Lavrik,O.I. (2013) Interaction of PARP-2 with DNA structures mimicking DNA repair intermediates and consequences on activity of base excision repair proteins. *Biochimie*, **95**, 1208–1215.
41. Audebert,M., Salles,B. and Calsou,P. (2004) Involvement of poly(ADP-ribose) polymerase-1 and XRCC1/DNA ligase III in an alternative .route for DNA double-strand breaks rejoining. *J. Biol. Chem.*, **279**, 55117–55126.
42. Beck,C., Boehler,C., Guirouilh Barbat,J., Bonnet,M.E., Illuzzi,G., Ronde,P., Gauthier,L.R., Magroun,N., Rajendran,A., Lopez,B.S. *et al.* (2014) PARP3 affects the relative contribution of homologous recombination and nonhomologous end-joining pathways. *Nucleic Acids Res.*, **42**, 5616–5632.
43. Lin,L., Zhang,Y.D., Chen,Z.Y., Chen,Y. and Ren,C.P. (2016) The clinicopathological significance of miR-149 and PARP-2 in hepatocellular carcinoma and their roles in chemo/radiotherapy. *Tumour Biol.*, **37**, 12339–12346.
44. Kang,Y.H., Lee,K.A., Kim,J.H., Park,S.G. and Yoon,D.Y. (2010) Mitomycin C modulates DNA-double strand break repair genes in cervical carcinoma cells. *Amino Acids*, **39**, 1291–1298.
45. Boudra,M.T., Bolin,C., Chiker,S., Fouquin,A., Zaremba,T., Vaslin,L., Biard,D., Cordelieres,F.P., Megnin-Chanet,F., Favaudon,V. *et al.* (2015) PARP-2 depletion results in lower radiation cell survival but cell line-specific differences in poly(ADP-ribose) levels. *Cell. Mol. Life Sci.*, **72**, 1585–1597.
46. Robert,I., Dantzer,F. and Reina-San-Martin,B. (2009) Parp1 facilitates alternative NHEJ, whereas Parp2 suppresses IgH/c-myc translocations during immunoglobulin class switch recombination. *J. Exp. Med.*, **206**, 1047–1056.
47. Bertrand,P., Akhmedov,A.T., Delacote,F., Durrbach,A. and Lopez,B.S. (1999) Human POMp75 is identified as the pro-oncoprotein TLS/FUS: both POMp75 and POMp100 DNA homologous pairing activities are associated to cell proliferation. *Oncogene*, **18**, 4515–4521.
48. Dumay,A., Laulier,C., Bertrand,P., Saintigny,Y., Lebrun,F., Vayssiere,J.L. and Lopez,B.S. (2006) Bax and Bid, two proapoptotic Bcl-2 family members, inhibit homologous recombination, independently of apoptosis regulation. *Oncogene*, **25**, 3196–3205.
49. Pierce,A.J., Johnson,R.D., Thompson,L.H. and Jasin,M. (1999) XRCC3 promotes homology-directed repair of DNA damage in mammalian cells. *Genes Dev.*, **13**, 2633–2638.
50. Forment,J.V., Walker,R.V. and Jackson,S.P. (2012) A high-throughput, flow cytometry-based method to quantify DNA-end resection in mammalian cells. *Cytometry A*, **81**, 922–928.
51. Chen,J., Ghorai,M.K., Kenney,G. and Stubbe,J. (2008) Mechanistic studies on bleomycin-mediated DNA damage: multiple binding modes can result in double-stranded DNA cleavage. *Nucleic Acids Res.*, **36**, 3781–3790.
52. Gibson,B.A., Zhang,Y., Jiang,H., Hussey,K.M., Shrimp,J.H., Lin,H., Schwede,F., Yu,Y. and Kraus,W.L. (2016) Chemical genetic discovery of PARP targets reveals a role for PARP-1 in transcription elongation. *Science*, **353**, 45–50.
53. Carter-O'Connell,I., Jin,H., Morgan,R.K., David,L.L. and Cohen,M.S. (2014) Engineering the substrate specificity of ADP-ribosyltransferases for identifying direct protein targets. *J. Am. Chem. Soc.*, **136**, 5201–5204.
54. Riccio,A.A., Cingolani,G. and Pascal,J.M. (2016) PARP-2 domain requirements for DNA damage-dependent activation and localization to sites of DNA damage. *Nucleic Acids Res.*, **44**, 1691–1702.
55. Carter-O'Connell,I. and Cohen,M.S. (2015) Identifying direct protein targets of poly-ADP-ribose polymerases (PARPs) using engineered PARP variants-orthogonal nicotinamide adenine dinucleotide (NAD+) analog pairs. *Curr. Protoc. Chem. Biol.*, **7**, 121–139.
56. Isabelle,M., Moreel,X., Gagne,J.P., Rouleau,M., Ethier,C., Gagne,P., Hendzel,M.J. and Poirier,G.G. (2010) Investigation of PARP-1, PARP-2, and PARG interactomes by affinity-purification mass spectrometry. *Proteome Sci.*, **8**, 22.
57. Guirouilh-Barbat,J., Huck,S., Bertrand,P., Pirzio,L., Desmaze,C., Sabatier,L. and Lopez,B.S. (2004) Impact of the KU80 pathway on NHEJ-induced genome rearrangements in mammalian cells. *Mol. Cell*, **14**, 611–623.
58. Yang,Y.G., Cortes,U., Patnaik,S., Jasin,M. and Wang,Z.Q. (2004) Ablation of PARP-1 does not interfere with the repair of DNA double-strand breaks, but compromises the reactivation of stalled replication forks. *Oncogene*, **23**, 3872–3882.
59. Mansour,W.Y., Borgmann,K., Petersen,C., Dikomey,E. and Dahm-Daphi,J. (2013) The absence of Ku but not defects in classical non-homologous end-joining is required to trigger PARP1-dependent end-joining. *DNA Repair (Amst.)*, **12**, 1134–1142.
60. Cruz-Garcia,A., Lopez-Saavedra,A. and Huertas,P. (2014) BRCA1 accelerates CtIP-mediated DNA-end resection. *Cell Rep.*, **9**, 451–459.
61. Polato,F., Callen,E., Wong,N., Faryabi,R., Bunting,S., Chen,H.T., Kozak,M., Kruhlak,M.J., Reczek,C.R., Lee,W.H. *et al.* (2014) CtIP-mediated resection is essential for viability and can operate independently of BRCA1. *J. Exp. Med.*, **211**, 1027–1036.
62. Sartori,A.A., Lukas,C., Coates,J., Mistrik,M., Fu,S., Bartek,J., Baer,R., Lukas,J. and Jackson,S.P. (2007) Human CtIP promotes DNA end resection. *Nature*, **450**, 509–514.
63. Isono,M., Niimi,A., Oike,T., Hagiwara,Y., Sato,H., Sekine,R., Yoshida,Y., Isobe,S.Y., Obuse,C., Nishi,R. *et al.* (2017) BRCA1

directs the repair pathway to homologous recombination by promoting 53BP1 dephosphorylation. *Cell Rep.*, **18**, 520–532.
64. Densham,R.M., Garvin,A.J., Stone,H.R., Strachan,J., Baldock,R.A., Daza-Martin,M., Fletcher,A., Blair-Reid,S., Beesley,J., Johal,B. *et al.* (2016) Human BRCA1-BARD1 ubiquitin ligase activity counteracts chromatin barriers to DNA resection. *Nat. Struct. Mol. Biol.*, **23**, 647–655.
65. Alagoz,M., Katsuki,Y., Ogiwara,H., Ogi,T., Shibata,A., Kakarougkas,A. and Jeggo,P. (2015) SETDB1, HP1 and SUV39 promote repositioning of 53BP1 to extend resection during homologous recombination in G2 cells. *Nucleic Acids Res.*, **43**, 7931–7944.
66. Bouwman,P., Aly,A., Escandell,J.M., Pieterse,M., Bartkova,J., van der Gulden,H., Hiddingh,S., Thanasoula,M., Kulkarni,A., Yang,Q. *et al.* (2010) 53BP1 loss rescues BRCA1 deficiency and is associated with triple-negative and BRCA-mutated breast cancers. *Nat. Struct. Mol. Biol.*, **17**, 688–695.
67. Biehs,R., Steinlage,M., Barton,O., Juhasz,S., Kunzel,J., Spies,J., Shibata,A., Jeggo,P.A. and Lobrich,M. (2017) DNA double-strand break resection occurs during non-homologous end joining in G1 but is distinct from resection during homologous recombination. *Mol. Cell*, **65**, 671–684.
68. Hu,Y., Wang,C., Huang,K., Xia,F., Parvin,J.D. and Mondal,N. (2014) Regulation of 53BP1 protein stability by RNF8 and RNF168 is important for efficient DNA double-strand break repair. *PLoS One*, **9**, e110522.
69. Jiang,G., Plo,I., Wang,T., Rahman,M., Cho,J.H., Yang,E., Lopez,B.S. and Xia,F. (2013) BRCA1-Ku80 protein interaction enhances end-joining fidelity of chromosomal double-strand breaks in the G1 phase of the cell cycle. *J. Biol. Chem.*, **288**, 8966–8976.
70. Zhong,Q., Chen,C.F., Chen,P.L. and Lee,W.H. (2002) BRCA1 facilitates microhomology-mediated end joining of DNA double strand breaks. *J. Biol. Chem.*, **277**, 28641–28647.
71. Luijsterburg,M.S., de Krijger,I., Wiegant,W.W., Shah,R.G., Smeenk,G., de Groot,A.J., Pines,A., Vertegaal,A.C., Jacobs,J.J., Shah,G.M. *et al.* (2016) PARP1 links CHD2-mediated chromatin expansion and H3.3 deposition to DNA repair by non-homologous end-joining. *Mol. Cell*, **61**, 547–562.
72. Polo,S.E., Kaidi,A., Baskcomb,L., Galanty,Y. and Jackson,S.P. (2010) Regulation of DNA-damage responses and cell-cycle progression by the chromatin remodelling factor CHD4. *EMBO J.*, **29**, 3130.
73. Ahel,D., Horejsi,Z., Wiechens,N., Polo,S.E., Garcia-Wilson,E., Ahel,I., Flynn,H., Skehel,M., West,S.C., Jackson,S.P. *et al.* (2009) Poly(ADP-ribose)-dependent regulation of DNA repair by the chromatin remodeling enzyme ALC1. *Science*, **325**, 1240–1243.
74. Bothmer,A., Robbiani,D.F., Feldhahn,N., Gazumyan,A., Nussenzweig,A. and Nussenzweig,M.C. (2010) 53BP1 regulates DNA resection and the choice between classical and alternative end joining during class switch recombination. *J. Exp. Med.*, **207**, 855–865.
75. Fradet-Turcotte,A., Canny,M.D., Escribano-Díaz,C., Orthwein,A., Leung,C.C., Huang,H., Landry,M.-C., Kitevski-LeBlanc,J., Noordermeer,S.M. and Sicheri,F. (2013) 53BP1 is a reader of the DNA-damage-induced H2A Lys 15 ubiquitin mark. *Nature*, **499**, 50–54.
76. Acs,K., Luijsterburg,M.S., Ackermann,L., Salomons,F.A., Hoppe,T. and Dantuma,N.P. (2011) The AAA-ATPase VCP/p97 promotes 53BP1 recruitment by removing L3MBTL1 from DNA double-strand breaks. *Nat. Struct. Mol. Biol.*, **18**, 1345–1350.
77. Botuyan,M.V., Lee,J., Ward,I.M., Kim,J.-E., Thompson,J.R., Chen,J. and Mer,G. (2006) Structural basis for the methylation state-specific recognition of histone H4-K20 by 53BP1 and Crb2 in DNA repair. *Cell*, **127**, 1361–1373.
78. Drané,P., Brault,M.-E., Cui,G., Meghani,K., Chaubey,S., Detappe,A., Parnandi,N., He,Y., Zheng,X.-F. and Botuyan,M.V. (2017) TIRR regulates 53BP1 by masking its histone methyl-lysine binding function. *Nature*, **543**, 211–216.
79. Mallette,F.A., Mattiroli,F., Cui,G., Young,L.C., Hendzel,M.J., Mer,G., Sixma,T.K. and Richard,S. (2012) RNF8- and RNF168-dependent degradation of KDM4A/JMJD2A triggers 53BP1 recruitment to DNA damage sites. *EMBO J.*, **31**, 1865–1878.
80. Chroma,K., Mistrik,M., Moudry,P., Gursky,J., Liptay,M., Strauss,R., Skrott,Z., Vrtel,R., Bartkova,J., Kramara,J. *et al.* (2017) Tumors overexpressing RNF168 show altered DNA repair and responses to genotoxic treatments, genomic instability and resistance to proteotoxic stress. *Oncogene*, **36**, 2405–2422.
81. Zhang,H., Liu,H., Chen,Y., Yang,X., Wang,P., Liu,T., Deng,M., Qin,B., Correia,C., Lee,S. *et al.* (2016) A cell cycle-dependent BRCA1–UHRF1 cascade regulates DNA double-strand break repair pathway choice. *Nat. Commun.*, **7**, 10201.